

## Supporting Information for

### Accurate Heteronuclear Distance Measurement under All Magic-Angle Spinning Frequencies in Solid-State NMR Spectroscopy

Lixin Liang<sup>1,2</sup>, Yi Ji<sup>1,2</sup>, Zhenchao Zhao<sup>1</sup>, Caitlin M. Quinn<sup>3</sup>, Xinhe Bao<sup>1</sup>, Tatyana Polenova<sup>3</sup>, Guangjin Hou<sup>1\*</sup>

<sup>1</sup>State Key Laboratory of Catalysis, National Laboratory for Clean Energy, 2011-Collaborative Innovation Center of Chemistry for Energy Materials, Dalian Institute of Chemical Physics, Chinese Academy of Sciences, Zhongshan Road 457, Dalian 116023, China.

<sup>2</sup>University of Chinese Academy of Sciences, Beijing 100049, China.

<sup>3</sup>Department of Chemistry and Biochemistry, University of Delaware, Newark, Delaware 19716, United States

Corresponding author: [ghou@dicp.ac.cn](mailto:ghou@dicp.ac.cn) (G.H.)

#### Table of contents

Supplementary Information	Page
Figure S1. The simulated effect of <sup>1</sup> H CSA in DIPSHIFT.	S2
Figure S2. The simulated effect of RF mismatch and MAS fluctuation	S2
Figure S3. Comparisons of wPMRR to other methods at 10 kHz MAS	S3
Figure S4. The simulations for windowed SR4.	S3
Figure S5. <sup>13</sup> C and <sup>15</sup> N NMR spectra and assignments of U- <sup>13</sup> C, <sup>15</sup> N-fMLF.	S3
Figure S6. Experiments and fitting curves of U- <sup>13</sup> C, <sup>15</sup> N-fMLF.	S4
Figure S7. The FID and FT lineshapes of <sup>1</sup> H- <sup>15</sup> N wPMRR-DIPSHIFT	S5
Figure S8. 1D <sup>31</sup> P MAS and 2D <sup>1</sup> H- <sup>31</sup> P HETCOR NMR spectra	S5
Figure S9. <sup>1</sup> H- <sup>31</sup> P PMRR-REDOR and <sup>31</sup> P- <sup>1</sup> H PMRR-DIPSHIFT of TMPO/HZSM-5	S6

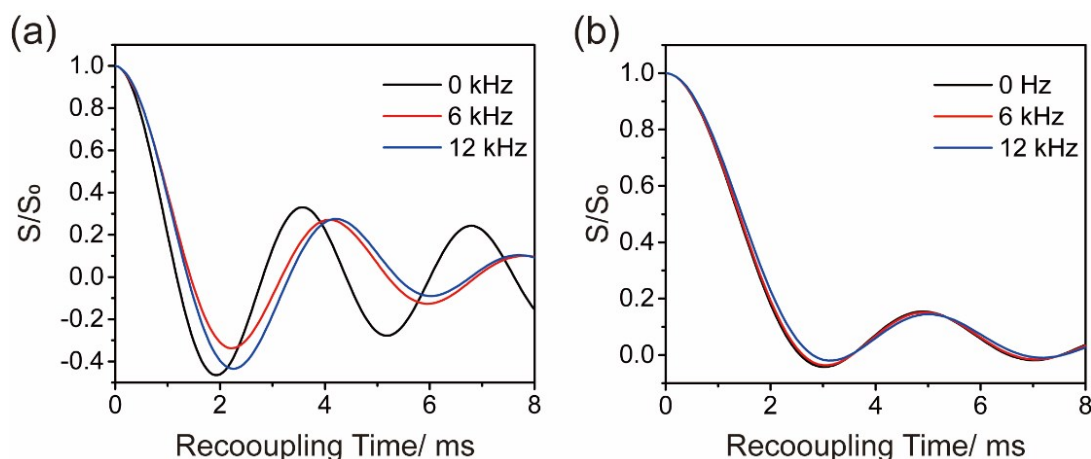


**Figure S1.** The simulated effect of  $^1\text{H}$  CSA on  $^1\text{H}$ - $^{13}\text{C}$  dipolar evolutions using (a)  $\text{R}^3$ - and (b) PMRR-based DIPSHIFT sequences. The observation spin is  $^{13}\text{C}$ . Three different values of  $^1\text{H}$  CSA were chosen, with black lines for  $\delta_\sigma = 0$  kHz, red lines for 6 kHz, blue lines for 12 kHz. Simulations were carried out at 16 kHz MAS and 14.10 T  $B_0$  field.

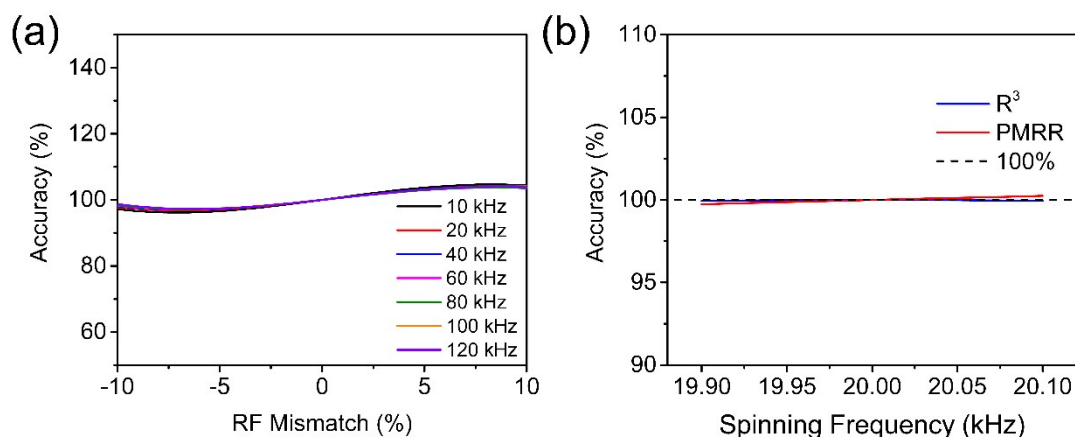


**Figure S2.** The simulated effect of (a) RF mismatch, in percentage, measured accuracy by  $^1\text{H}$ - $^{15}\text{N}$  DCC PMRR sequence at MAS rates from 10 to 120 kHz; (b) fluctuation of spinning frequency at MAS rate of 20 kHz.

From Figure S2a, it's clear that the curves from all these spinning frequencies are almost identical, which indicates that the effect of RF mismatch **in percentage** is independent to the MAS conditions. However, in practical application, the same percentage of RF mismatch at faster MAS rates corresponds to much larger amplitude deviation in kHz, and it's more reasonable to evaluate the robustness to RF mismatch **in kHz**, while RF inhomogeneity **in percentage**. Simulations were carried out at 14.10 T  $B_0$  field.

From Figure S2b, under  $\pm 100$  Hz fluctuation around 20 kHz spinning frequency, although the PMRR is slightly less stable than the  $\text{R}^3$ , its variation of accuracy caused by the fluctuation is still negligible ( $< 0.3\%$ ).

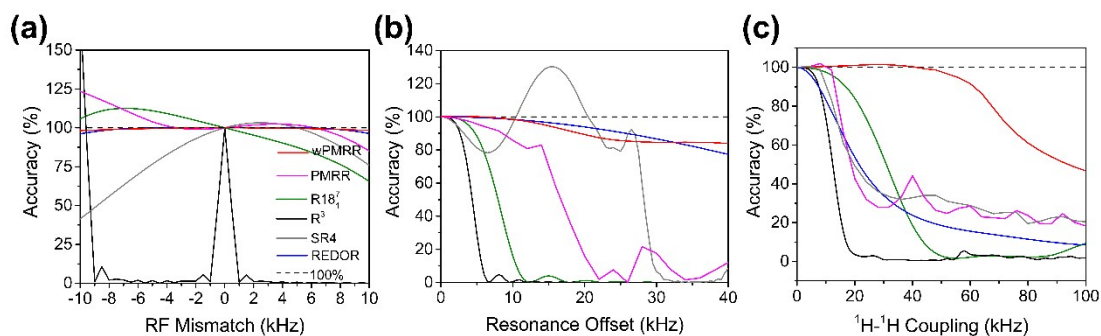


**Figure S3.** Comparisons of wPMRR ( $f_w = 0.8$ , presented by red line) to other methods under the interferences of (a) RF mismatch; (b) resonance offset; (c)  $^1\text{H}$ - $^1\text{H}$  coupling.

Other methods are PMRR (windowless, purple),  $R18_1^7$  (green),  $R^3$  (black), SR4 (grey) and REDOR (blue). The  $R18_4^1$  in Figure 1 is replaced by  $R18_1^7$ , since  $R18_1^7$  is more suitable at 10 kHz MAS. The RF amplitude of REDOR recoupling sequence is 80 kHz.

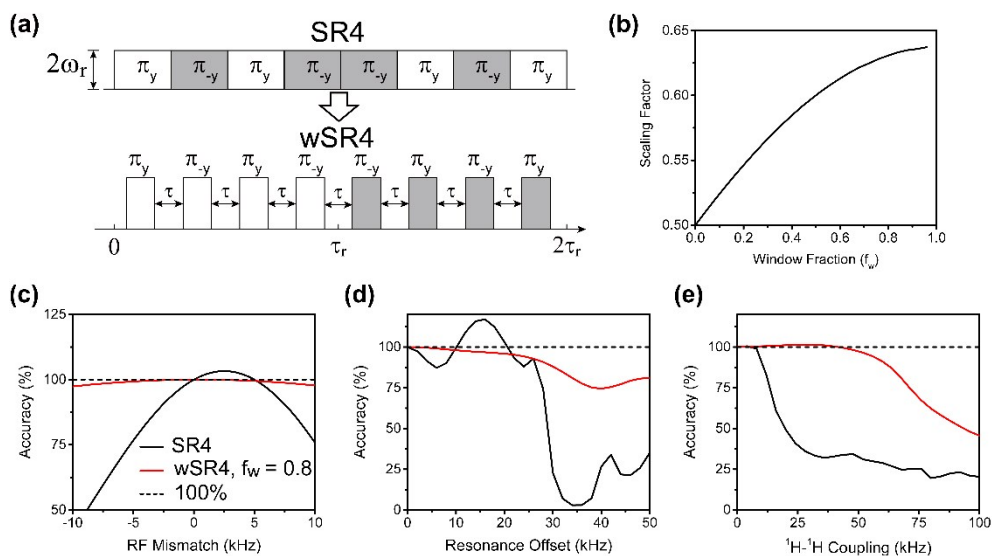


**Figure S4.** (a) Pulse sequence of windowed SR4, white rectangles denote  $\pi$  pulses with  $90^\circ$  phase, and grey rectangles denote  $\pi$  pulses with  $270^\circ$  phase; (b) Scaling factor of wSR4 as a function of window fraction ( $f_w$ ); Performance comparisons between SR4 and windowed SR4 with  $f_w = 0.8$  at MAS rate of 10 kHz for the tolerance to (c) RF mismatch, (d) resonance offset, (e)  $^1\text{H}$ - $^1\text{H}$  dipolar coupling.

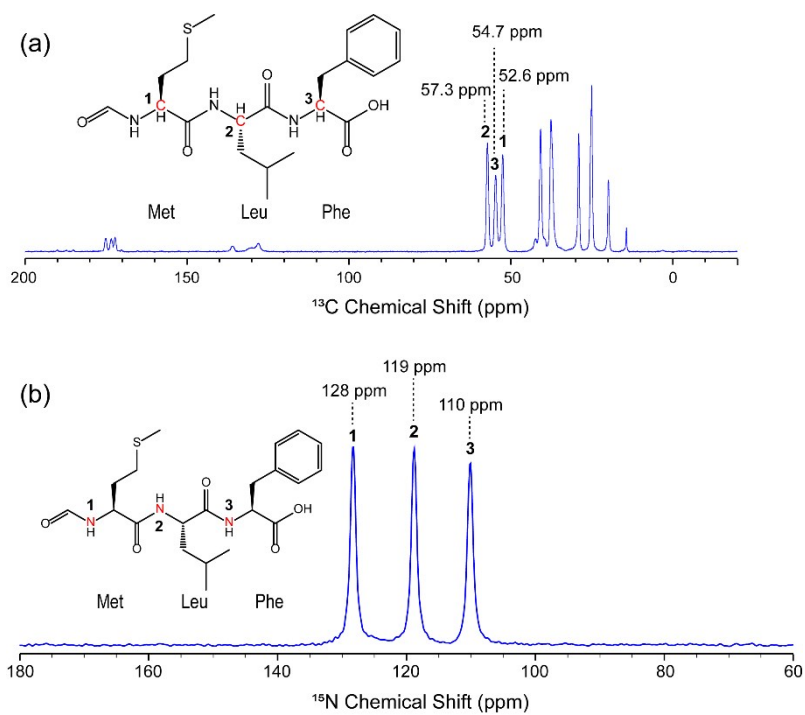


**Figure S5.** 1D (a) <sup>13</sup>C and (b) <sup>15</sup>N CP/MAS NMR spectra of U-<sup>13</sup>C, <sup>15</sup>N-fMLF acquired at 20 kHz MAS and 14.1 T.

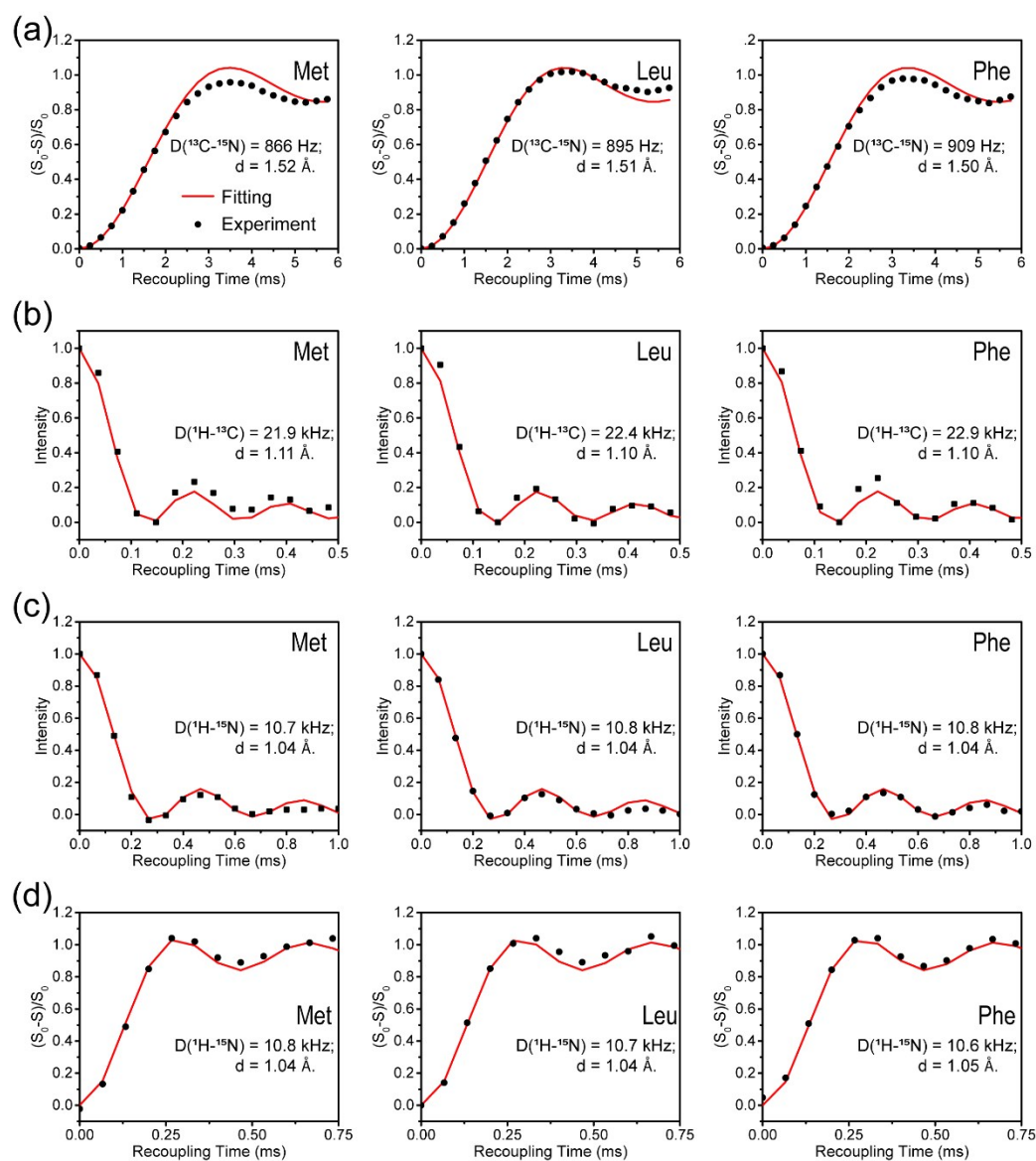


**Figure S6.** The experimental (black dots) and fitted (red lines) (a)  $^{13}\text{C}_\alpha\text{-}^{15}\text{N}$  PMRR-REDOR, (b)  $^1\text{H}\text{-}^{13}\text{C}_\alpha$  PMRR-DIPSHIFT, (c)  $^1\text{H}\text{-}^{15}\text{N}$  PMRR-DIPSHIFT and (d)  $^1\text{H}\text{-}^{15}\text{N}$  PMRR-REDOR in  $\text{U}\text{-}^{13}\text{C}$ ,  $^{15}\text{N}\text{-fMLF}$ . The fitting parameters, i.e., DCCs and the corresponding internuclear distances, are also shown in each figure.

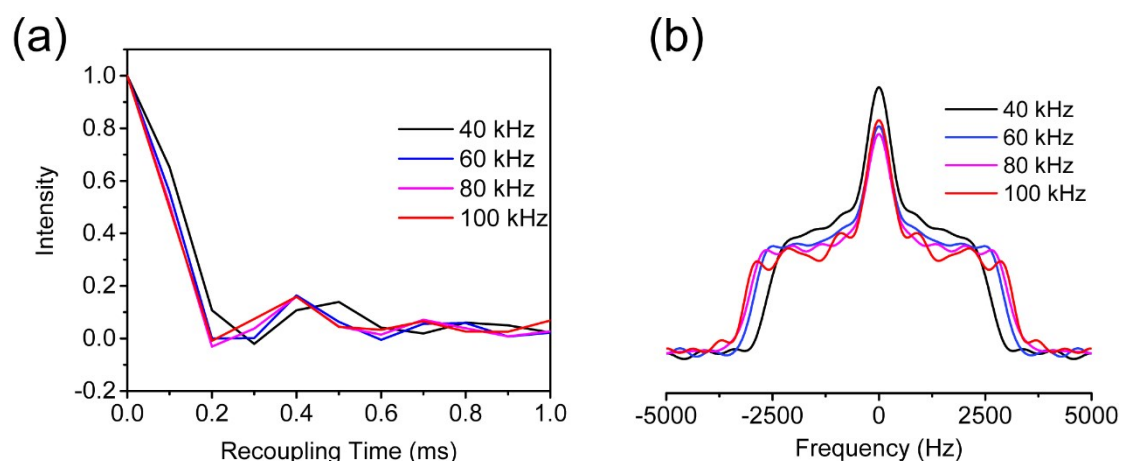


**Figure S7.** The extracted (a) dipolar evolution (FID) in F1 dimension and (b) the Fourier transformed lineshapes in  $^1\text{H}$ - $^{15}\text{N}$  wPMRR-DIPSHIFT experiment of U- $^{13}\text{C}$ ,  $^{15}\text{N}$ -fMLF at MAS rate of 20 kHz, with the recoupling RF field strength of 40 kHz ( $f_w = 0.00$ , black), 60 kHz ( $f_w = 0.33$ , blue), 80 kHz ( $f_w = 0.50$ , purple) and 100 kHz ( $f_w = 0.60$ , red).

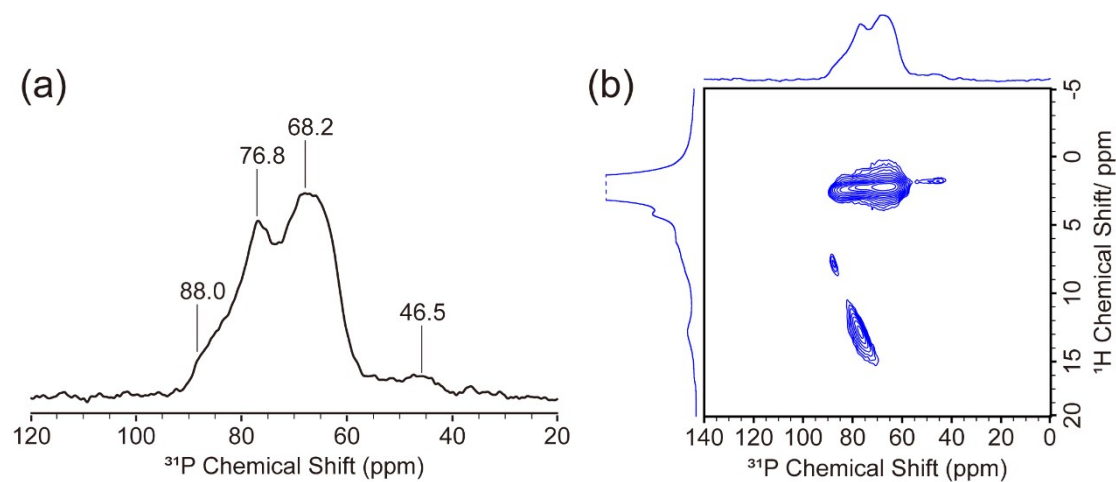


**Figure S8.** (a)  $^{31}\text{P}$  NMR spectrum of TMPO adsorbed on H-ZSM-5, the sample is labeled as TMPO/HZSM-5. (b) The 2D  $^{31}\text{P}$ - $^1\text{H}$  HETCOR of TMPO/HZSM-5.

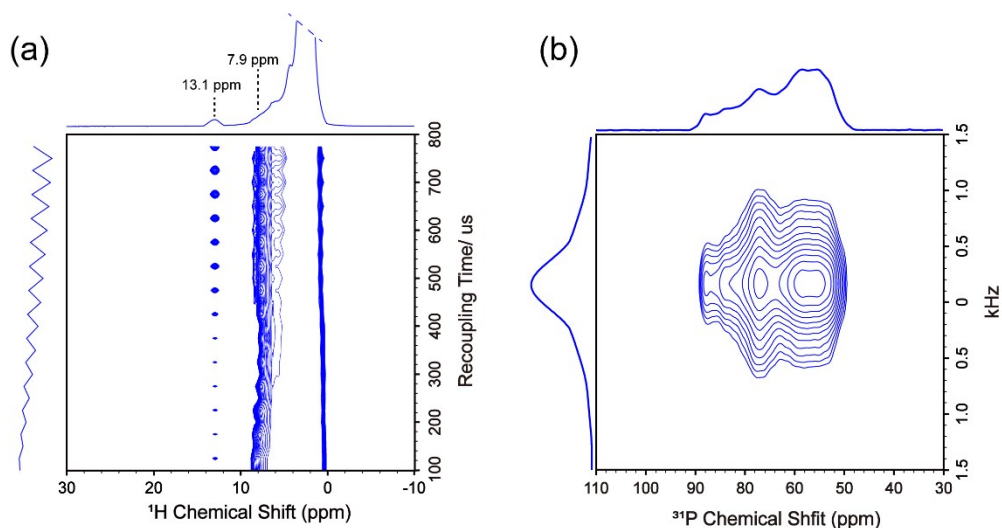


**Figure S9.** (a) Pseudo 2D NMR spectrum of  $^1\text{H}$ - $^{31}\text{P}$  PMRR-REDOR with  $^1\text{H}$  detection, where interleaved  $S_0$  and  $S$  were recorded in the indirect dimension. The extraction of  $^1\text{H}$ - $^{31}\text{P}$  dipolar dephasing for  $^1\text{H}$  signal at 7.9 ppm is obscured by serious overlapping with  $^1\text{H}$  at 6~9 ppm. (b) 2D  $^{31}\text{P}$ - $^1\text{H}$  PMRR-DIPSHIFT spectrum with  $^{31}\text{P}$  detection. The Fourier transformed lineshapes overlapped severely, hampering the extraction of  $^{31}\text{P}$ - $^1\text{H}$  DCCs.